



Technical note

Estimating dynamic skin tension lines in vivo using 3D scans[☆]Hyewon Seo^{a,*}, See-jo Kim^b, Frederic Cordier^c, Jiyoung Choi^d, Kyunghi Hong^d^a University of Strasbourg (UMR 7005 CNRS), Boulevard S. Brant, F-67400 Illkirch, France^b Andong National University, Republic of Korea^c LMIA, Université de Haute-Alsace, France^d Department of Clothing and Textiles, Chungnam National University, Republic of Korea

ARTICLE INFO

Keywords:

Langer's line
Computer aided analysis
Skin tension
3D-scan data

ABSTRACT

Skin tension lines, defined as the lines of maximal tension, often provide guidelines for surgical incisions and pattern design of tight-fit, functional clothing. In this work, we are interested in developing methods for finding personalized, dynamic skin tension lines (DSTL) in a non-invasive manner. We base our study on the kinematic analysis of point markers that are colored on the skin. By tracking the motion-induced displacement of point markers, we locally analyze the skin deformation and numerically compute the maximum tension directions. Then, finding DSTL is transformed to the problem of finding continuous, interpolating locally computed lines of the maximum tension directions. Compared to existing methods, our method involves less invasive measurement on the skin, and is equipped with computational methods for identifying dynamic skin tension automatically. Consequently, our method is convenient to carry out, less prone to erroneous measurement, and repeatable. Our experiments have been successfully carried out on, though not limited to, lower body skins of male subjects.

© 2012 Elsevier Ltd. All rights reserved.

1. Introduction

Langer's line is a term used to define the direction within the human skin along which the skin has maximum tension. It is named after Langer, who punctured numerous holes at short distances from each other into the skin of a cadaver with an awl that had a circular-shaped tip, and noticed that the resultant punctures in the skin had ellipsoidal shapes. From this testing he determined "line directions" by smoothly connecting the longer axes of the ellipsoidal holes [1]. These lines, which are also termed as "cleavage lines", show the directions of greatest skin tension. The surgical importance of Langer's lines has been first noted by Kocher [2]. He advised that surgical incisions are carried out in the direction of Langer's lines, because the scars would be least conspicuous and heal better. Since then, many surgeons have searched for the ideal guide to use for elective incisions, and there exist more than thirty differently named guidelines today [3].

One problem with Langer's line has been that they represent lines of cleavage in cadavers and not lines of relaxed skin

tension. Indeed, the facial musculature of a cadaver is often not relaxed, as some display a wide-eyed stare or wide-open mouth. Accordingly, surgeons have investigated less invasive methods to determine relaxed skin tension lines in-vivo, among them are Kraissl's lines [2] and relaxed skin tension lines [4]. Kraissl's line coincides with wrinkle lines, although not always, and tend to be perpendicular to the muscle action. Thus, Kraissl's lines are found by studying the direction of underlying muscle fiber. Relaxed skin tension lines [4,5] are the tension lines which follow the furrows formed when the skin is relaxed. In practice, they are derived from the act of pinching the skin and observing the furrows and ridges that are formed. Pinching parallel to the resting skin tension lines results in fewer and higher furrows than if it were done in the perpendicular direction. Although this method can provide personalized guidelines for elective incisions relatively easily, it may be subjective and may not be convenient, as it requires pinching.

We note that most of these lines are static in nature. That is, forces causing the tension on the skin are inherent in the skin or the body contents itself and not related to muscular action. However, surgeons and scientists agree that skin tension is dependent not only on the enclosed body content but also on joint movements. Similarly to the static tension lines, dynamic skin tension lines (DSTL) are defined as the maximum tension lines formed when the muscles are in action. To the best of our knowledge, the first work on the dynamic tension lines are by Bush et al. [6], who have measured the orientation of maximal strains on different location

[☆] This work has been supported by Specific & Fundamental Research Program (No. 2009-0083874) of Korean National Research Foundation. The first author has been partly supported by the Imagerie et Robotique Médicale et Chirurgicale (IRMC) program and by the project SHARED (No. 10-CHEX-014-01) funded by French National Research Agency.

* Corresponding author.

E-mail address: seo@unistra.fr (H. Seo).



Fig. 1. Prior to the 3-D scan, we place color markers on the skin of the subject (left). Screenshot of 3-D laser scans of a subject at various poses (knee flexion angles of 0°, 30°, 45°, and 60°) (right).

of the face with five different facial expressions. However, their experiments have been based on the excision of naevi from the face and neck, which is invasive and requires multiple subjects in order to be able to cover the entire face area.

The primary objective of this research is estimating personalized dynamic skin tension lines *in vivo*, in a non-invasive manner. We base our study on the kinematic analysis of point markers that are colored on the skin. By tracking the motion-induced displacement of point markers, we locally analyze the skin deformation and numerically compute the maximum tension directions. Then, finding DSTL is transformed to the problem of finding continuous, interpolating lines of the maximum tension directions. Smooth, continuous dynamic skin tension lines have been drawn on the skin surface by adopting interpolation and path-line integral over the marker meshes. Based on computational methods, our method is convenient to carry out, less prone to erroneous measurement, and repeatable. Our experiments have been carried out on, though not limited to, the skin on the legs of male subjects.

2. Data acquisition

A whole body 3-D range scanner [7] has been used to capture the shape of the subject as well as to track the location change of landmarks in the skin. Prior to the scan, red-colored circular landmarks, whose diameters are approximately 1 cm, have been regularly placed on the skin, approximately 2–3 cm apart. Fig. 1 shows the screenshots of range scans taken on two subjects holding four different postures. In order to analyze the skin deformation on the legs during knee bending action, we have chosen the postures with different knee flexion angles of 0°, 30°, 45°, and 60°. The flexion angles have been measured by the angle between the femur and tibia bones, by using a goniometer.

3. Marker extraction and labeling

We take the scanned mesh data as input and begin by separating the marker triangles from the rest of the skin mesh. Since the markers are drawn by colors that are clearly distinguishable (red) from that of the skin or of the underwear, we can easily identify marker triangles by using a color key. We locate each vertex in the color space as defined by the HSV (Hue-Saturation-Value) color model. We first map the color of each triangle vertex to the color space defined by the HSV the hexagonal cone. We then define marker regions in the hexagonal cone, based on the thresholds of H (5°–10°) and S (7%–12%) values. If all three vertices of a triangle fall into the marker region, then we consider that triangle constitutes a marker and label it as marker triangle. If one or two vertices belong

to the marker region, we query if the center of the triangle falls into the marker region. If it is the case, it is classified as marker triangle.

Note that the mesh generated from the scanner is highly dense, and each marker is typically composed of dozens of marker triangles. In order to determine the 3-D coordinate of a marker center from a set of marker triangles, we cluster the triangles into groups according to their proximity. Initially we start with groups each containing one marker triangle. Then groups are merged together if they are located within certain distance (1 cm, the diameter of the circular marker). We repeat this merging process several times until no more groups are merged. To this end, triangles belonging to the one group are considered to constitute one marker together. The center of mass of each cluster is taken as the 3-D coordinate of the corresponding marker.

Next, we proceed with the marker labeling. This is important as the same marker must be identified across multiple scans taken with different poses of the same subject. Assuming that the number of extracted markers are identical among all scans of the same subject, the problem of marker labeling amounts to solving an assignment (LAP) problem. To this end, we employ the Hungarian method [8,9], a universal solver for LAP. The sum of distances among the corresponding markers has been used as the cost function to be minimized. For complete description of the Hungarian method readers may refer to the Munkres' paper [9].

The matching algorithm works well when the numbers of markers are similar and when there actually exist matching pairs for the majority of markers. When the number of markers are largely different from each other, that is to say, when the marker extraction does not work well for some parts in either of the scan data, the matching fails mostly for those whose corresponding pairs had not been extracted. The most problematic case occurs when the number of markers are similar but the corresponding pairs are missing for both scan data. On the average the rate of successful matching was 90.83%.

4. Triangle-based strain computation

We have devised a triangle based strain analysis method, by embedding a set of virtual strain gages on each triangle. Plain strain components located on the three dimensional surface can also be obtained by a conventional finite element method (FEM) [10,11]. However, if we consider large deformation we should take care of nonlinear terms as well as subject-specific material properties of the skin. Moreover, the simulation requires very small time step, implying long computation time. Thus, the method of strain gage rosettes has been adopted. One difference compared with previous work is that each strain gage rosettes is constructed by connecting one marker to each of the other markers, and to their center in the

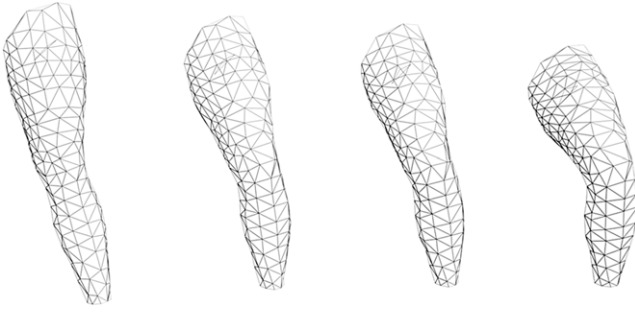


Fig. 2. Triangle mesh generated from the marker data. Note that the topologies of these meshes are identical across the same subject, so that we can carry out strain analysis on each triangle by comparing its changes with knee flexion.

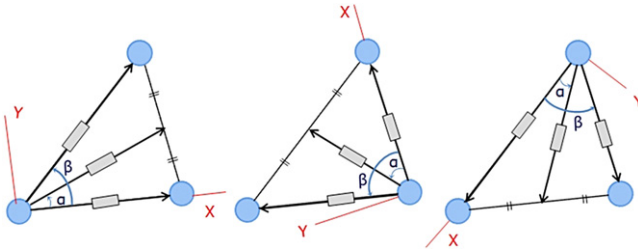


Fig. 3. Three virtual strain gage rosettes, each connecting its center to a triangle vertex, are embedded on a deformable triangle. To simplify the computation, the X-axis is aligned with the first virtual strain gage. The principal strain directions computed from this setting are guaranteed to be tangential to the surface.

triangle element, which has not been introduced before. For each labeled set of markers, we first obtain a triangle mesh by using the existing method of Ball-Pivoting algorithm [12]. Starting with a seed triangle, a ball of a user-specified radius pivots around an edge until it touches another point, forming another triangle. The process iteratively continues until all reachable edges have been tried, and then starts from another seed triangle, until all points have been considered. As a result, we obtain a mesh composed of triangles connecting the markers, which we call as marker mesh. Note that it is sufficient to run the triangulation only once for each subject – since the markers from the same subjects are labeled across different poses, the same triangle index can be used for both the initial and the deformation configurations. These are referred to as initial marker mesh and deformed marker mesh, respectively (Fig. 2).

Now we have the triangle meshes that are topologically consistent across different postures of the same subject. In order to compute principal strain directions, we consider for each triangle three sets of virtual strain gage rosettes, as shown in (see Fig. 3). Each strain gage rosettes is constructed by connecting one marker to each of the other markers, and to their center. Each of the linear strain gage of the gage rosettes is named A, B, and C, in a counter-clockwise order. From the lengths of the linear strain gage A as measured before and after the deformation, noted as e_A and e'_A respectively, we obtain the engineering strain $\epsilon_A = (e'_A - e_A)/e_A$. ϵ_B and ϵ_C are obtained similarly.

The transformation of engineering strains ϵ_A , ϵ_B , and ϵ_C to normal (ϵ_X and ϵ_Y) and shear strains (γ_{XY}) is accomplished with the basic equations for a three-gage strain gage rosette [6]:

$$\begin{aligned} \epsilon_A &= \frac{\epsilon_X + \epsilon_Y}{2} + \frac{\epsilon_X - \epsilon_Y}{2} \cos(2 \times 0) + \frac{\gamma_{XY}}{2} \sin(2 \times 0), \\ \epsilon_B &= \frac{\epsilon_X + \epsilon_Y}{2} + \frac{\epsilon_X - \epsilon_Y}{2} \cos(2 \times \alpha) + \frac{\gamma_{XY}}{2} \sin(2 \times \alpha), \\ \epsilon_C &= \frac{\epsilon_X + \epsilon_Y}{2} + \frac{\epsilon_X - \epsilon_Y}{2} \cos(2 \times \beta) + \frac{\gamma_{XY}}{2} \sin(2 \times \beta) \end{aligned} \quad (1)$$

where α represents the angle between the first and second linear gages, and β between the first and third ones. Note that the normal and shear strains are specific to the coordinate system, in which the x-axis is aligned with the first linear strain gage.

Now that we have computed for each triangle 3 sets of normal and shear strains that are defined in different coordinate systems, we proceed with the computation of principal strains from each set and the average of them in a global coordinate system. A 2 by 2 matrix is composed with diagonal elements ϵ_X and ϵ_Y , and off-diagonal symmetric elements $\epsilon_{XY} = \gamma_{XY}/2$. The first eigenvector (and its eigenvalue) of the matrix corresponds to the maximum strain direction (and its magnitude). Note that principal strains equal to zero mean no-deformation. Therefore, the sign of the principal strains being greater and less than zero, indicates elongation and compression of the skin during the motion, respectively.

5. Extraction of DSTL

Our goal is now to compute smooth, continuous lines interpolating the maximal strain directions on each triangle. Note the task of DSTL extraction is related to but slightly different from tensor visualization [13], given with this specific goal of obtaining continuous lines on the skin surface. Assuming that the strain directions do not change abruptly between neighboring triangles, we adopt a vector-field based method to compute the smooth, continuous dynamic skin tension lines on the skin surface. That is to say, a three-dimensional vector-field \mathbf{v} over the skin surface is approximated using the maximal strain directions calculated at each vertex. Then, the DSTLs are obtained by computing pathlines of particles moving on the skin through a pathline integral, assuming the velocity of each particle governed by \mathbf{v} . The line integral is appropriate for our purpose since it guarantees no overlap between different paths. As an analogy to the relaxed skin tension lines, we consider that it is the direction they convey that is important, and that there is no fixed number of lines or separation spaces between them.

We first let the user to select a number of points p_{src} on the skin surface, and compute pathlines starting from each of these points. A pathline of the vector field \mathbf{v} starting from p_{src} is a function $(p(t))$ solution of the following set of equations:

$$\begin{cases} \frac{d}{dt}p(t) = \mathbf{v}(p(t)) & \text{for } t \in [0, t_{trg}] \\ p(0) = p_{src} \end{cases} \quad (2)$$

t_{trg} is a variable which allows the user to modify the length of the pathline. The pathline $p(t)$ starting from a point p_{src} is the trajectory that this point would make as it moves with the flow of the vector field defined by the principal strain directions; at any time, $\frac{d}{dt}p(t)$, the tangent vector at $p(t)$, is equal to $\mathbf{v}(p(t))$ the value of the vector field at the location of $p(t)$. The pathline integral is appropriate for our purpose since (1) it coincides with the principal direction at the marker location and smoothly interpolates in between, and (2) it guarantees no overlap between different paths.

To solve Eq. (2), we use the 4th order Runge–Kutta integration with adaptive step-size. One integration step involves computing an approximation of the vector field $\mathbf{v}(p(t))$ and the intermediate solution $p(t + \delta t)$, δt being the time step. The approximation of the vector field at the location of $p(t)$ is computed as follows: we first find the skin mesh triangle T in which $p(t)$ is located. We then compute α_i , α_j and α_k , the three barycentric coordinates corresponding to the three vertices v_i , v_j and v_k of T . The value of the vector field is

$$\mathbf{v}(p(t)) = \alpha_i \cdot \mathbf{v}(v_i) + \alpha_j \cdot \mathbf{v}(v_j) + \alpha_k \cdot \mathbf{v}(v_k). \quad (3)$$

$\mathbf{v}(v_i)$, $\mathbf{v}(v_j)$ and $\mathbf{v}(v_k)$ are the principal strain directions at v_i , v_j and v_k respectively.

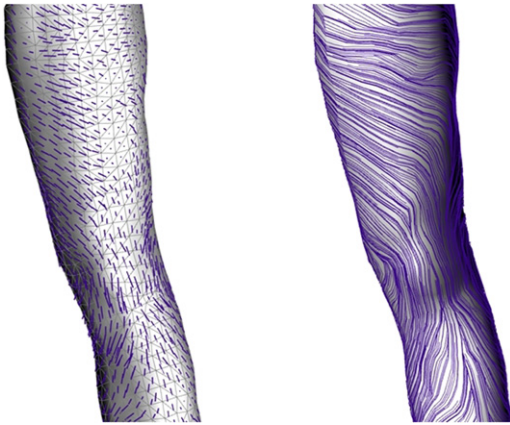


Fig. 4. Orientation of the lines of maximum strain on the anterior leg surface during the knee bending action. Indicated by the short lines at the center of each triangle (left), the lines point in the direction in which the skin stretches and contracts the maximum during knee bending. DSTL (right) is extracted by computing the tangent curve of the vector field.

6. Results

We have tested our method on three young males of different physical characteristics (thick, standard, and thin). In Fig. 4, we show the results of strain analysis and DSTL that we obtained by applying the proposed method on a thin male subject. Fig. 6 shows the maximal strain tension and dynamic tension lines we obtained for these subjects at 30 (left column), 45 (middle column), and 60 (right column) degrees of knee flexion. The degree of maximal strain tension is encoded as a colormap. The bending action resulted in dynamic skin tension in all sites on the leg. Below we summarize our findings.

- The highest degree of strain tension was observed near the patella and the knee hollow. Inner side of the front thigh also showed relatively high magnitudes.
- As the bending angle increases, the principal strain values also become higher. The principal strain directions, however, remain relatively unchanged over the knee bending.
- There exists interpersonal variation on DSTL.
- Commonalities can be easily found across individuals: all DSTLs have longitudinal orientation over the patella, transverse orientation on the knee hollow, and diagonal orientation on the thigh, both on the front and on the back (from upper-medial to lower-lateral).

The proposed algorithms have been implemented on an Intel Core2 Duo 2.53 GHz CPU running on Windows XP operating system. The computation of principal strains and DSTL took about 0.17 s and 10.1 s, respectively, for a mesh composed of 894 vertices and 1784 triangles. The time complexities of both algorithms are linear, that is, the computation time increases proportionally to the number of triangles in the mesh.

7. Discussion

Since our algorithm is the first one tailored for the dynamic skin tension lines, it is difficult to perform any fair comparisons. Moreover, most of the known lines require invasive experiments involving incisions on the skin, which is beyond the scope of this study. Nevertheless, comparing DSTL with other known lines may give some insights on the characteristics of DSTL. Here we provide visual comparisons with Langer's lines and Kraissle's lines. RSTLs have been excluded from the comparison because it is mostly used for the face, rather than the body [3]. By comparing Langer's lines (Fig. 5 (left)) to our DSTL (Fig. 6), similarities can be seen on the

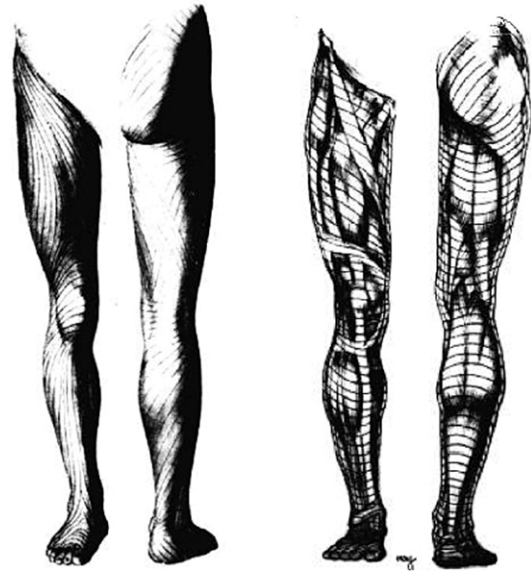


Fig. 5. Langer's lines (left) and Kraissle's lines (right) on the leg [2].

knee hollow, where the lines are all horizontal. As well, similar boundary line (diagonal from the crotch to the lateral side of the knee) can be noted on the upper posterior thigh. In most of the other regions, Langer lines and DSTL tend to be perpendicular to each other. On the patella, for instance, while Langer lines have transverse orientation, DSTL are oriented rather longitudinal over the patella, on all subjects. Similarly, on the thigh, Langer lines are diagonal connecting the upper-lateral part to the lower-medial part of the thigh, whereas DSTL connect the upper-medial part to the lower-lateral part. Although arguable, Kraissle's lines (Fig. 5 (right)) show rather perpendicular orientations to our DSTLs on most of the regions on the leg, except for the knee hollow region.

8. Conclusion and limitations

We have demonstrated in this work how laser scanning technology can be used to measure the dynamic skin tension lines, i.e. the direction of skin tension caused by muscle actions such as knee flexion. By tracking the motion-induced displacement of marker points on the skin surface, the three components of the orthogonal strain tensor and the directions of maximum strain were computed for three representative male samples. The developed triangle-based strain analysis and the combined method of interpolation and path line integral allow characterizing the directions of maximum dynamic skin strain, in an efficient and repeatable manner. Equipped with automatic computation algorithms, our method is less invasive, efficient, and can be used to find personalized dynamic tension lines. Compared to most existing methods for extracting skin tension lines, our method addresses the dynamic tension lines on the body. In addition, our DSTL is less invasive, more efficient, and more comfortable to obtain than existing lines. We expect that our result will be useful for applications such as surgical planning, and medical dressing.

There are a number of assumptions used in our setting. First, we assume that the body in motion is sufficiently approximated with data containing only the initial and final states of the movement. Since our data is obtained from a high quality 3-D scanning device, which requires about 10 s for each scan, the frame rates we can get is rather limited. Second, the error inherent to the laser scanning is considered tolerable, although sometimes noticeable error may be found in the scan data depending on the scanning resolution of the device and involuntary movement of the subject during the scanning.

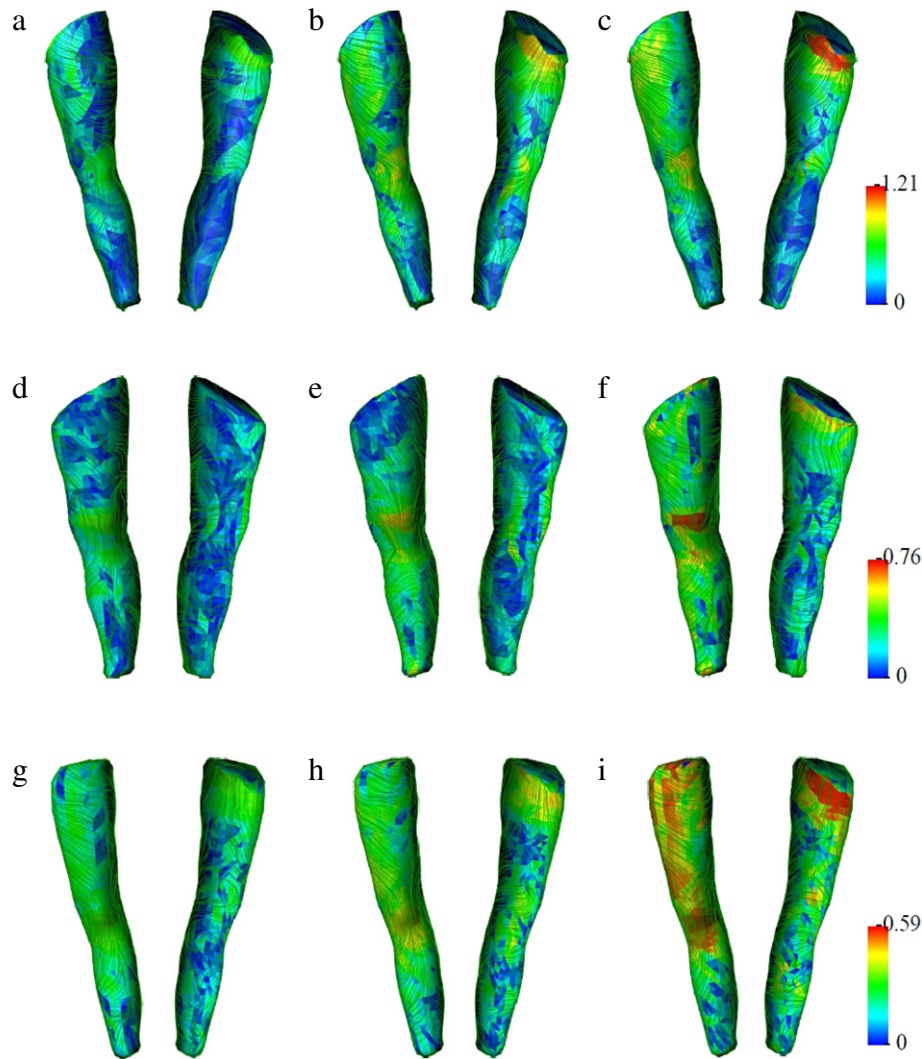


Fig. 6. DSTLs obtained on three different subjects and poses. From left to right: DSTL with 30° (left), 45° (middle), and 60° (right) of knee bending. From top to bottom: DSTLs of standard (top), thick (middle), and thin (bottom) male bodies. For each image pair, the image on the left depicts the front view and on the right the back view.

One shortcoming of our method is that it requires drawing a large number of color markers on the skin, which may not be very practical as the surface area becomes large. Still, drawing markers on the skin does not require special skill and can easily be parallelized by several operators, since our method does not impose any particular constraints on the spatial arrangements of these markers.

References

- [1] Gibson T. Karl Langer and his lines. *Br J. Plast. Surg.* 1978;31:1–2.
- [2] Kraissl CJ. The selection of appropriate lines for elective surgical incisions. *Plastic and Reconstructive Surgery* 1951;8(1):1–28.
- [3] Wilhelmi BJ, Blackwell SJ, Phillips LG. Langers lines: to use or not to use. *Plastic and Reconstructive Surgery* 1999;104(1):208–14.
- [4] Borges AF. Relaxed skin tension lines (RSTL) versus other skin lines. *Plastic and Reconstructive Surgery* 1984;73(1):144–50.
- [5] Borges AF. Relaxed skin tension lines. *Dermatologic Clinics* 1989;7(1):169–77.
- [6] Crandall SH, Dahl NC, Larder TJ. *An introduction to the mechanics of solids*. 2nd ed. McGraw-Hill; 1978.
- [7] Whole Body Color 3D Scanner, Cyberware, <http://www.cyberware.com/products/scanners/wbx.html>.
- [8] Kuhn HW. The Hungarian method for the assignment problem. *Naval Research Logistics Quarterly* 1955;2:8397.
- [9] Munkres J. Algorithms for the assignment and transportation problems. *Journal of the Society for Industrial and Applied Mathematics* 1957;5(1):3238.
- [10] Wayne FLarrabe. A finite element model of skin deformation. I. *Biomechanics of skin and soft tissue: a review*. *The Laryngoscope* 1986;96(4):399–405.
- [11] Flynn C, McCormack BAO. A simplified model of scar contraction. *Journal of Biomechanics* 2008;41(7):1582–9.
- [12] Bernardini F, Mittleman J, Rushmeier H, Silva C, Taubin G. The Ball–Pivoting algorithm for surface reconstruction. *IEEE Transactions on Visualization and Computer Graphics* 1999;5(4):349–59.
- [13] Weickert J, Hagen H. *Visualization and processing of tensor fields*. Springer; 2006.